Scientific Research Publishing

Atmospheric and Climate Sciences, 2025, 15(3), 615-644
https://www.scirp.org/journal/acs
ISSN Online: 2160-0422
ISSN Print: 2160-0414

Infrared Backradiation under Low Humidity Conditions: An Evaluation of Greenhouse Gas Impact

Ernst Hammel, Martin Steiner, Robert Glaubauf

International Climate Research, A Citizen Research Group, Vienna, Austria
Email: ernst@icr2025.org, steiner@icr2025.org, robert.glaubauf@intelligentsoftware.at

How to cite this paper: Hammel, E., Steiner, M. and Glaubauf, R. (2025) Infrared Backradiation under Low Humidity Conditions: An Evaluation of Greenhouse Gas Impact. *Atmospheric and Climate Sciences*, **15**, 615-644.
https://doi.org/10.4236/acs.2025.153031

Received: April 23, 2025
Accepted: June 21, 2025
Published: June 24, 2025

Abstract

This study examines the impact of greenhouse gases (GHG) on infrared back radiation (IRBR) in extreme desert and midlatitude winter conditions. Employing MODTRAN simulations, pyrgeometer measurements and energy balance fit models, we assess the impacts of CO_2, Argon (Ar), N_2O and R-134a. Results indicate that increasing CO_2 concentrations yield a very limited additional IRBR effect, whereas R-134a exhibits significant radiative forcing even at trace levels. These findings highlight the critical role of synthetic GHGs in climate dynamics and provide insights into radiative forcing in arid regions, enhancing climate model accuracy for desert environments and contribute to the general assessment of the impact of increasing CO_2 concentrations in our atmosphere. Likewise, these measurements have shown again that the contribution of CO_2 to the total back radiation is largely saturated within the historical concentration boundaries far beyond current levels and back radiation by water vapor is the dominant effect.

Keywords

Infrared Back Radiation, Desert Climate, Radiative Forcing, Energy Balance, Greenhouse Gases, Arid Regions, Humidity

1. Introduction

Radiative processes play a central role in the Earth's energy balance, influencing both local weather patterns and the global climate system [1]-[3]. The Earth's surface receives incoming shortwave radiation from the Sun, which is partially

reflected and absorbed by the surface, while longwave (infrared) radiation is emitted back into the atmosphere and space. This balance of incoming and outgoing radiation regulates temperature and drives atmospheric dynamics, making the accurate understanding of radiative processes essential for climate studies [4] [5].

Incoming radiation refers to the solar radiation that reaches the earth's surface and atmosphere. About 30% of this radiation is reflected back into space due to the atmosphere and earth albedo, and the remaining 70% is absorbed by the atmosphere, land, and oceans [6]. The earth's surface absorbs this energy, which warms the surface and contributes to evaporation, convection, photosynthesis, and other critical processes that drive weather and climate.

NASA's CERES (Clouds and the Earth's Radiant Energy System) mission provides extensive data on this component, with measurements of the Earth's energy budget. CERES provides precise observations of incoming solar radiation at different latitudes, times of day, and seasons. Using CERES data allows to monitor variations in incoming shortwave radiation and assess how much energy is absorbed by the surface or reflected by clouds and aerosols [7]-[9].

To assess the radiative forcing of CO_2 and TFE (Tetrafluoroethane) under field conditions we studied radiation flux data obtained from satellite-based observations in the CERES_EBAF-TOA_Edition4.1 database. This edition includes precise global measurements of energy fluxes at the top of atmosphere (TOA), which are essential for calculating radiative forcing. Our analysis focused on the database's ability to capture variations in atmospheric composition and their influence on the radiative budget specifically during December, a month characterized by distinct seasonal changes in radiative properties, when we started the series of measurements.

Figure 1 illustrates the changes over a year timespan in the comparative areas of interest within the radiative budgets as obtained by CERES. Dryer conditions in the winter season allows more upwelling LW radiation to escape the atmospheric absorption and encouraged us to use the month of December to study CO_2 forcing effects at the White Desert Camp in Egypt.

Reflected Shortwave Radiation is the fraction of incoming solar radiation reflected mainly by the clouds and to lesser degrees by ice and snow and other surface features, expressed by the albedo, which varies also depending on surface types (e.g., forests, deserts, oceans, cities), controlling the amount of reflection. Higher albedo (e.g., ice-covered regions) reflects more solar radiation, while lower albedo (e.g., dark ocean surfaces) absorbs more [6].

Longwave (Infrared) Radiation is emitted by the Earth and its atmosphere as thermal energy. The Earth's surface emits infrared radiation that is partially absorbed and re-emitted by the atmosphere (especially by greenhouse gases like water vapor and carbon dioxide), leading to the greenhouse effect. Some of the longwave radiation escapes directly into space, and some is returned to the surface as infrared back radiation [1].

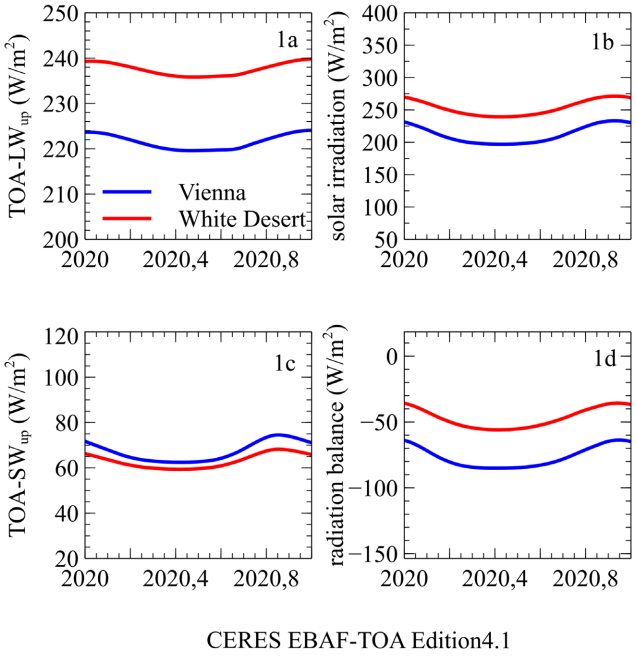

Figure 1. (a) Upwelling TOA longwave radiation at Vienna (Austria) and White Desert (Egypt); (b) Solar irradiation at Vienna (Austria) and White Desert (Egypt); (c) Upwelling TOA shortwave radiation at Vienna (Austria) and White Desert (Egypt); (d) Radiation balance at Vienna (Austria) and White Desert (Egypt). All data are from CERES_EBAF-TOA_Edition4.1 for the period of January 2020 until December 2020 [7]-[9].

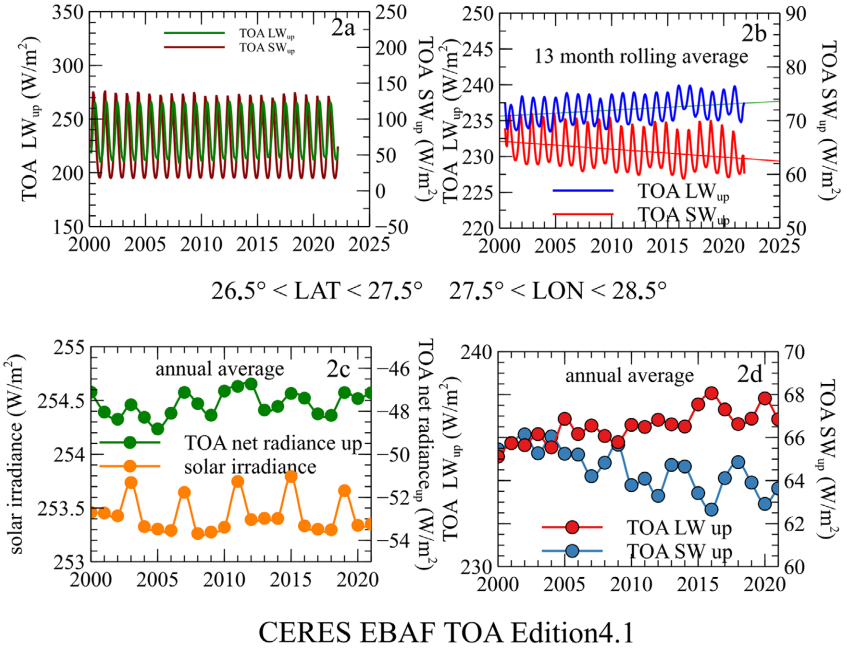

Figure 2. (a) White Desert upwelling TOA longwave (LW) and upwelling TOA shortwave (SW) radiation; (b) White Desert 13 month rolling average upwelling TOA LW and upwelling TOA SW radiation; (c) White Desert annual average for upwelling TOA LW and upwelling TOA SW radiation; (d) White Desert annual average for radiation balance and solar irradiance. All data are from CERES_EBAF-TOA_Edition4.1 for the period of March 2000 until February 2022 [7]-[9].

It is useful to compare the CERES desert data above with CERES Vienna area data. Figures 1-3 analyze in more detail the differences of radiative properties

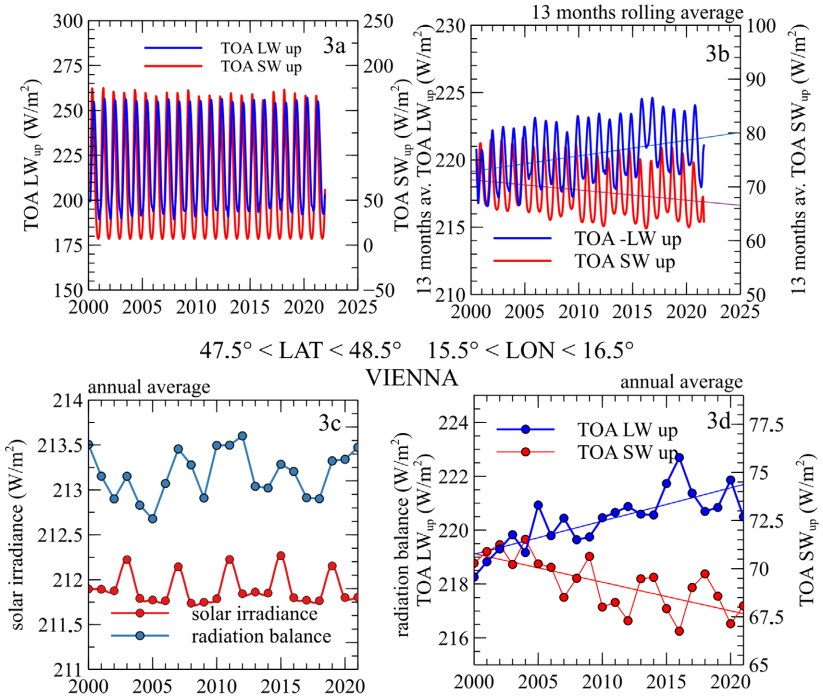

Figure 3. (a) Vienna area upwelling TOA longwave (LW) and upwelling TOA shortwave (SW) radiation; (b) Vienna area 13 month rolling average upwelling TOA LW and upwelling TOA SW radiation; (c) Vienna area annual average for upwelling TOA LW and upwelling TOA SW radiation; (d) Vienna area annual average for radiation balance and solar irradiance. All data are from CERES_EBAF-TOA_Edition4.1 for the period of March 2000 until February 2022 [7]-[9].

over the range of more than 20 years in the White Desert area and the Vienna area, as seen from remote satellite sensors. Infrared back radiation (IRBR) is a critical component of the Earth's energy balance, specifically related to the longwave radiation emitted from the atmosphere back toward the surface. This phenomenon significantly impacts surface temperature and, in turn, influences evaporation, convection, precipitation patterns, and the hydrological cycle. The amount of infrared radiation absorbed by the surface depends on factors such as the concentration of greenhouse gases, cloud cover, and surface properties like albedo and roughness [1]. Changes in the concentration of greenhouse gases or cloud cover can enhance or dampen the infrared radiation, which in turn affects global warming and regional climate patterns.

A low ratio LW/SW of upwelling TOA longwave radiation to solar irradiance (see Figure 4) is advantageous when measuring the radiative forcing of increased CO_2 because it indicates a more significant contribution from solar radiation relative to the upwelling TOA longwave radiation [6]. This allows for a more precise and sensitive measurement of the Earth's energy balance changes due to CO_2-induced radiative forcing. In such conditions, the influence of greenhouse gases like

CO_2 is more pronounced, as the additional longwave radiation absorbed and emitted by CO_2 contributes more notably to the alteration of the Earth's radiative energy budget. By minimizing the loss of longwave radiation relative to solar irradiance, it becomes easier to isolate the effects of CO_2 from other radiative influences, leading to a clearer and more accurate quantification of its radiative forcing impact. The arid desert and the smaller LW/SW ratio at this time of the year were the main motivation to make use of the given conditions in the White Desert in Egypt end of last December.

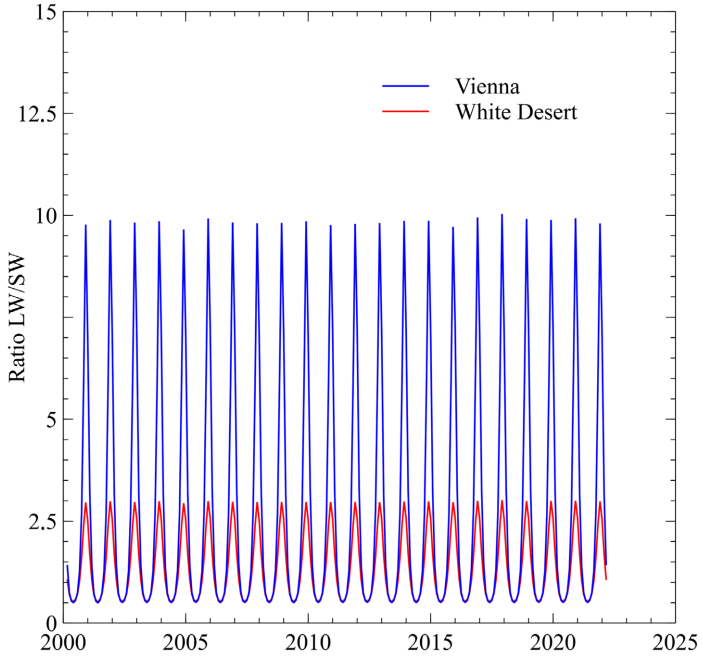

Figure 4. Ratio of upwelling TOA longwave radiation to solar irradiation LW/SW.

1.1. The Role of Deserts in Global Energy Exchange

Deserts are extreme environments that significantly impact global energy exchange. These regions are characterized by high solar radiation due to their mostly clear skies, which results in intensified daytime heating. At night, however, desert regions experience dramatic cooling due to the lack of water vapor and cloud cover, which normally traps heat in more humid environments. This extreme diurnal variation in temperature is largely governed by infrared radiative processes. The predominantly clear skies are the primary factor contributing to the lower TOA albedo levels influenced by surface albedo and atmospheric scattering compared to those in the Vienna region.

Deserts are known for low surface albedo (compare TOA SW_{up} in **Figure 2(d)** and **Figure 3(d)**), particularly in sand-dominated regions, which means that they absorb a significant amount of incoming shortwave radiation (**Figure 5**). However, their lack of vegetation and moisture leads to limited heat retention and rapid cooling at night. The emitted infrared radiation (**Figure 1(a)**, **Figure 2(a)** and **Figure 3(a)**) and the resulting infrared back radiation are key factors in this

process. At night, the surface of deserts cools rapidly due to the emission of infrared radiation into space, but the atmosphere also contributes by radiating infrared energy back to the surface, effectively reducing the amount of cooling [1].

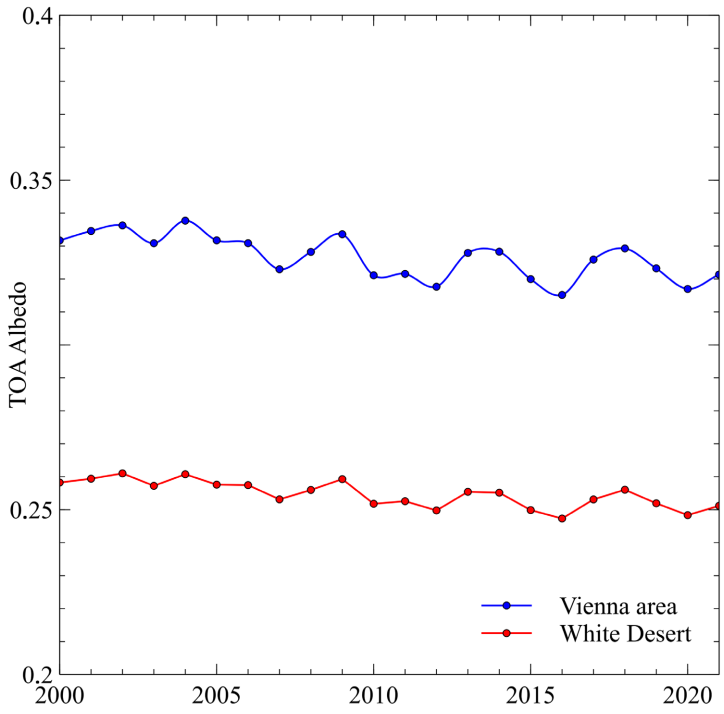

Figure 5. Comparison of albedo computed from CERES data [7]-[9].

The presence of desert regions significantly impacts the Earth's overall energy budget. Deserts contribute to both global warming and cooling processes, as they represent areas where high solar radiation is absorbed during the day and substantial cooling occurs at night. Accurate representation of infrared back radiation in these regions is essential for understanding the net energy flux and its impact on regional and global climate, as visible in NIMBUS data (**Figure 6**) [11].

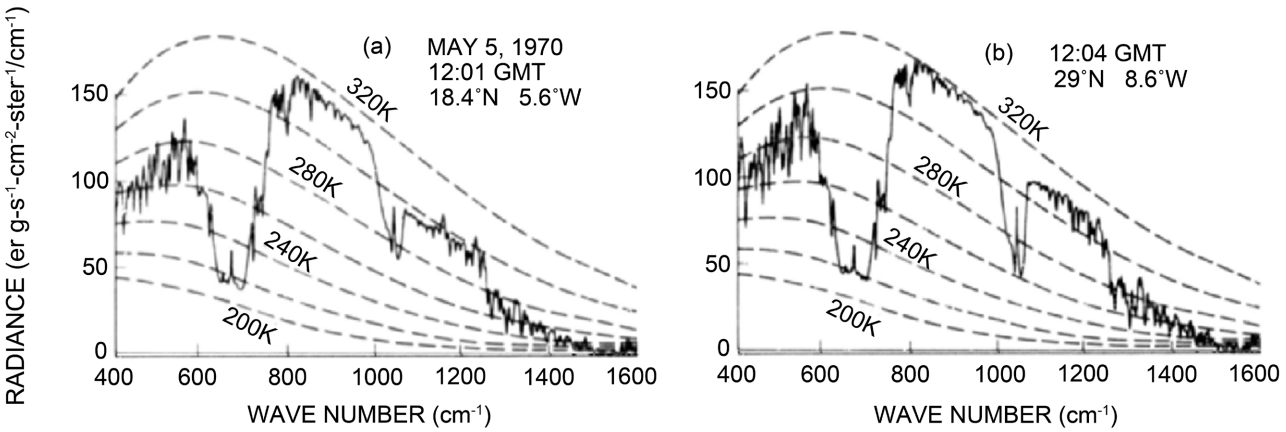

Figure 6. Examples of the historic NIMBUS mission spectra obtained over North Africa [11]. Blackbody curves for selected temperatures are included for comparison. Variations in the surface emissivity are apparent in the 1100 - 1200 cm^{-1} region.

Climate models are designed to simulate and forecast long-term climate trends, including temperature changes, precipitation patterns, and extreme weather events. However, the accuracy of these models heavily depends on how well they capture the radiative processes, particularly infrared back radiation, in different environments. Given that desert regions are underrepresented in many global climate models due to their sparse vegetation and extreme conditions, the accurate representation of radiative fluxes in these areas is critical for improving model predictions [12].

Infrared back radiation in deserts is influenced by a combination of factors, including surface temperature, atmospheric composition, and local cloud cover. As desert regions are subject to rapid changes in temperature often at low humidity, understanding how infrared radiation interacts with the atmosphere and surface is essential for accurately predicting desert climates. Furthermore, as deserts expand or contract in response to climate change, improving our understanding of infrared back radiation in these regions will be crucial for predicting their role in future global climate scenarios. The University of Chicago used MODTRAN to simulate some NIMBUS Sahara data (**Figure 7**) [13].

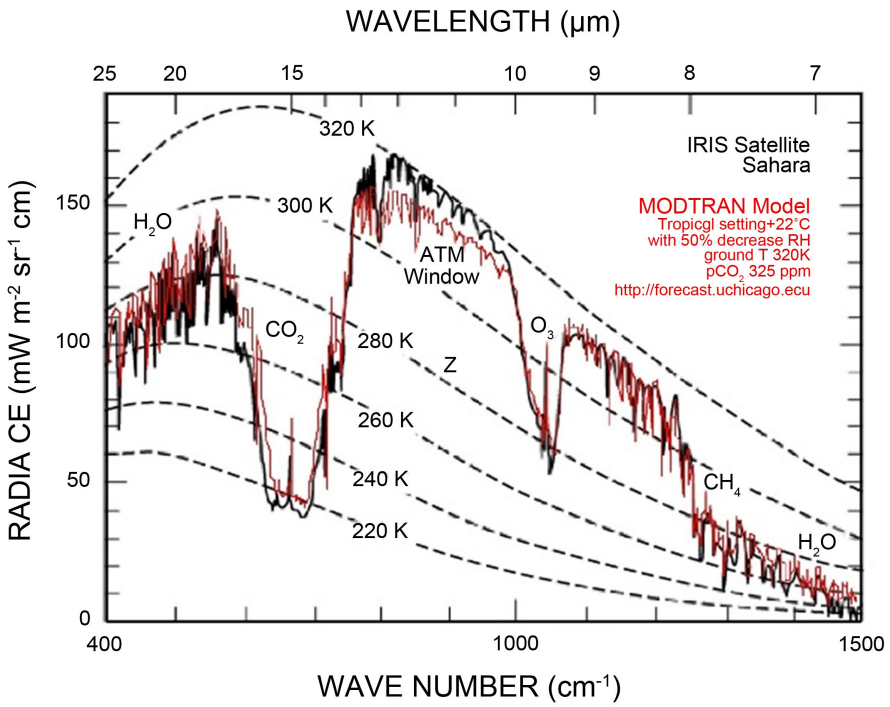

Figure 7. MODTRAN results (red) compared with data (solid black) from the Nimbus 3 IRIS instrument [11].

To compare results between local measurements and results obtained last December in the White Desert, located in the Farafra depression, 45 km north of the town of Qasr Al Farafra, we used the same choice of scenarios (tropical) as the University of Chicago, but at appropriate temperature offsets. As pointed out, deserts can act as significant sources of heat, especially during the daytime, which

can influence regional weather systems and contribute to the development of atmospheric instability. In turn, the nighttime infrared back radiation can have a mitigating effect on the diurnal temperature swing, influencing local and regional weather patterns. Understanding these dynamics also allows for more precise predictions of heat waves, droughts, and other climate events that are especially relevant in arid regions.

A study by Zhou and Wang examined the sensitivity of outgoing longwave radiation (OLR) and cooling rates to changes in far-infrared surface emissivity [10]. The research highlighted how variations in surface emissivity can significantly impact the radiative cooling of desert surfaces, thereby influencing the overall energy balance in these regions.

Zhou analyzed land surface temperature (LST) over global deserts, noting that deserts are less opaque to thermal infrared radiation due to minimal water vapor and cloud cover [14]. This characteristic leads to more pronounced diurnal temperature variations, affecting the infrared back radiation patterns observed in these areas.

Ogawa and Schmugge focused on estimating broadband emissivity in the thermal infrared region for desert areas [15]. Accurate emissivity values are essential for determining net longwave radiation and affecting infrared back radiation measurements. The research provided methodologies for mapping emissivity across extensive desert regions, contributing to a better understanding of their radiative properties.

Zhou discussed how deserts, due to their clear skies and minimal cloud cover, are less opaque to thermal infrared radiation [12]. This property makes them more sensitive to changes in atmospheric composition, such as increased CO_2 levels, leading to more pronounced warming effects compared to other regions.

In desert environments, extreme conditions like high temperatures, low humidity, and limited rainfall create a controlled and predictable system for studying increased CO_2 effects. With their clear skies and minimal cloud cover, deserts provide a consistent backdrop for studying infrared radiation, as there are fewer atmospheric variables (like humidity or cloud cover) to interfere with the measurements.

2. Methodology

We used a portable foiled test chamber to measure variations in infrared back radiation under high CO_2 concentrations, providing a controlled environment to isolate the effects of CO_2 and other greenhouse gases on atmospheric radiative properties. By trapping high CO_2 levels inside the chamber, we could directly assess its impact on the thermal radiation balance, ensuring that observed changes in infrared back radiation are primarily due to CO_2 variations, not other environmental factors. This makes the results more precise and focused, allowing for a clearer understanding of how CO_2 influences radiative forcing in a desert environment, as well as during the validation measurement at cold and cloudless winter days in midlatitude areas like Vienna.

2.1. Study Area

We chose the White Desert near Farafra in Egypt, located in the western part of the Egyptian Sahara around 500 km southwest of Cairo. This desert is an area of particular interest due to its distinct limestone formations and extreme climatic conditions, making it an ideal location for studying infrared back radiation under high CO_2 concentrations. The climate in this area is characterized by extreme arid conditions. It is part of the hyper-arid climate zone of the Sahara Desert. During the summer months (May to September), the White Desert experiences extreme heat, with daily maximum temperatures often surpassing 40˚C. The sun's intense radiation during the day creates significant infrared radiation flux, making it a perfect time to study the effects of CO_2 in the atmosphere, as the large temperature difference between day and night results in strong thermal radiation contrasts. Nighttime temperatures can be much cooler, with drops often reaching 5˚C - 15˚C. The transitional seasons (March to April, October) experience milder temperatures than summer but still maintain significant temperature differences between day and night. During these months, the variability in infrared back radiation is somewhat less extreme than in the summer but remains notable, with more moderate daytime highs and cooler nights. In the winter months (November to February), daytime temperatures can be more moderate, with highs around 20˚C - 25˚C. However, nighttime temperatures can still plummet, sometimes dropping to below 0˚C during cold spells. This seasonal variation creates a marked difference in infrared radiation during the night, with the cooler desert surface emitting less longwave radiation. Winter is typically drier, with even less rainfall than during other seasons, and the low humidity remains constant. The region averages less than 3 cm of rain per year, making it one of the driest places on Earth. The lack of moisture in the atmosphere further reduces the absorption of infrared radiation, enhancing the clarity of radiation measurements.

To provide a comparative dataset, we also conducted similar measurements in Vienna, Austria, under different climatic conditions. Unlike the White Desert, Vienna experiences a temperate climate with higher humidity levels and more frequent cloud cover, which can significantly impact infrared radiation flux. The seasonal temperature variations in Vienna are also less extreme, with milder differences between daytime and nighttime temperatures compared to the desert. This allowed us to analyze how CO_2-driven infrared back radiation behaves in an environment with increased atmospheric moisture and cloud presence, providing a contrasting dataset to the arid conditions of the White Desert.

The seasonal temperature fluctuations and minimal cloud cover in the White Desert create ideal conditions for studying infrared back radiation. The clear skies and low humidity mean there is minimal interference from water vapor, allowing for precise measurements of radiation fluxes. Furthermore, the stark temperature differences between day and night make it easier to assess radiative cooling and heating, both of which are strongly influenced by changes in CO_2 concentration. In Vienna, however, the presence of higher humidity and usually more cloud

cover provided insight into how these factors modulate infrared back radiation in a more humid and temperate setting.

In this study, the primary objective was to measure infrared radiation, specifically the additional infrared back radiation emitted from the atmosphere of the test chamber towards the surface under high CO_2 concentrations. To achieve accurate and reliable measurements, we utilized two identical Apogee Pyrgeometers, which are commonly employed for detecting longwave infrared radiation (4–50 μm), one to measure infrared radiation inside the test chamber and another one to measure the total hemispherical radiation outside. They provide high accuracy, with precision better than ±0.5% when exchanged against each other, ensuring reliable data under the varying experimental conditions in the test chamber. These instruments have a high sensitivity to small variations in infrared radiation, allowing for detection of minute changes in radiation flux due to altered CO_2 concentrations in the chamber. The same methodology was applied in both study locations to ensure consistency and comparability of results.

Prior to the experiment, they were calibrated by the manufacturer against a known radiation source to ensure accurate readings. Calibration is a critical step to account for any instrument-specific variations and ensure that the radiation flux measurements reflect the true values. Each detector was connected to a Data Acquisition System (DAQ) for collecting and recording the data. The DAQ system provided real-time monitoring of the radiation levels, allowing for continuous data logging throughout the experiment. The DAQ system is capable of high-frequency data collection, recording measurements at 1-second intervals, allowing for the observation of rapid changes in infrared radiation.

In this study, a portable UT A37 CO_2 Meter using Non-Dispersive Infrared (NDIR) technology was employed to monitor the concentration of carbon dioxide (CO_2) < 5000 ppm within the test chamber. This device was crucial in maintaining and recording the CO_2 levels required for the experiment, providing real-time data on gas concentrations that directly influence the infrared radiation measurements. Response times in the range of seconds allowed for continuous monitoring and immediate adjustment of CO_2 levels if required. This was particularly important under the dynamic experimental conditions, where gas concentrations may fluctuate due to ventilation or chamber adjustments.

The Non-Dispersive Infrared (NDIR) sensor detects CO_2 based on the absorption of infrared light at a wavelength specific to CO_2 molecules (around 4.26 μm). Other greenhouse gases having no strong absorption in this wavelength region can still be detected with much lower sensitivity if their transmittance is not 100%. In fact, the second gas (TFE) used in this experimental study has only a 90% transmittance in this wavelength range, leading to a detector cross-sensitivity of 10%.

The UT A37 CO_2 Meter was placed inside the test chamber, positioned at a representative location where it could measure the average concentration of CO_2 throughout the chamber. Continuous monitoring of the CO_2 concentration en-

sured that the chamber environment remained consistent for the duration of the experiment, allowing for precise assessment of how CO_2 influences infrared back radiation.

In addition to the infrared radiation measurements, Elitech portable, high-precision humidity and temperature data loggers were used to continuously monitor the environmental conditions within the test chamber. These instruments were important for tracking the temperature and humidity profiles at the bottom and top of the chamber, allowing us to evaluate how changes in CO_2 concentration might affect these parameters. Accurate measurement of temperature and humidity is crucial for understanding the dynamics of infrared back radiation and energy transfer in the chamber, particularly under elevated CO_2 conditions. The comparative measurements between the White Desert and Vienna provided a broader perspective on the role of atmospheric composition and climate in influencing infrared back radiation.

2.2. Data Collection

We used a skeleton made of metal or composite rods and wrapped it in one to two layers of PE-foils of 10μm thickness. This foil has approximately 90% transparency for short- and longwave radiation. In MODTRAN simulations, we attempted to account for the presence of the PE foil, which has its own IR absorption characteristics, by approximating its effect through a virtual increase in relative humidity. The primary similarity between the IR spectra of polyethylene and water arises in the C-H stretching (3000 - 2800 cm^{-1}) from -CH_2- groups, while Water has a strong, broad absorption band near 3200 - 3600 cm^{-1}, due to O-H stretching. The C-H bending of PE is around 720 and 1500 - 1300 cm^{-1}, while water shows H-O-H bending near 1640 cm^{-1}. So their infrared (IR) spectra can show some overlapping or analogous features due to the nature of molecular vibrations, but we understand our MODTRAN based estimations of their measurement impact as an intended simplification to account for existing thin foil effects. This is particularly arguable, as the IR absorption bands of water and polyethylene are close to each other or overlap.

To ensure the accuracy of our data, we conducted multiple test runs, comparing measurements with and without the PE-foil enclosure. This helped us quantify any potential deviations caused by the foil. The enclosure also provided a controlled environment, minimizing disturbances from wind and ensuring consistent atmospheric conditions within the chamber. Additionally, temperature and humidity profiles were closely monitored to evaluate the stability of experimental conditions, ensuring that any observed variations in IR back radiation could be confidently attributed to changes in CO_2 concentration rather than external influences.

The measurement series in Vienna used two identical test chambers, each with dimensions of 62 cm × 100 cm × 184 cm. These chambers were used to conduct parallel experiments, allowing for cross-verification of results and ensuring the reproducibility of our measurements. The use of identical chambers (see **Figure 8**

right side) minimized experimental uncertainties and provided a consistent basis for analyzing the effects of increased greenhouse gas concentrations on infrared back radiation.

In contrast, the single mobile test chamber (see Figure 8 left side) used in the desert was a cube with dimensions of 150 cm × 150 cm × 150 cm. This larger chamber design allowed for a more extensive volume of gas to be tested under the extreme climatic conditions of the White Desert. The increased internal volume also provided a more representative environment for assessing radiative energy transfer in an open, arid setting, where largely reduced presence of atmospheric moisture and cloud cover can significantly reduce the IR back radiation dynamics.

Both chamber configurations were designed to accommodate precise instrumentation, including pyrgeometers for measuring longwave infrared radiation, CO_2 sensors for tracking gas concentrations, and temperature and humidity data loggers. The structural integrity of the chambers helped to obtain more stable conditions throughout the measurement series, allowing for reliable data collection across different environmental settings.

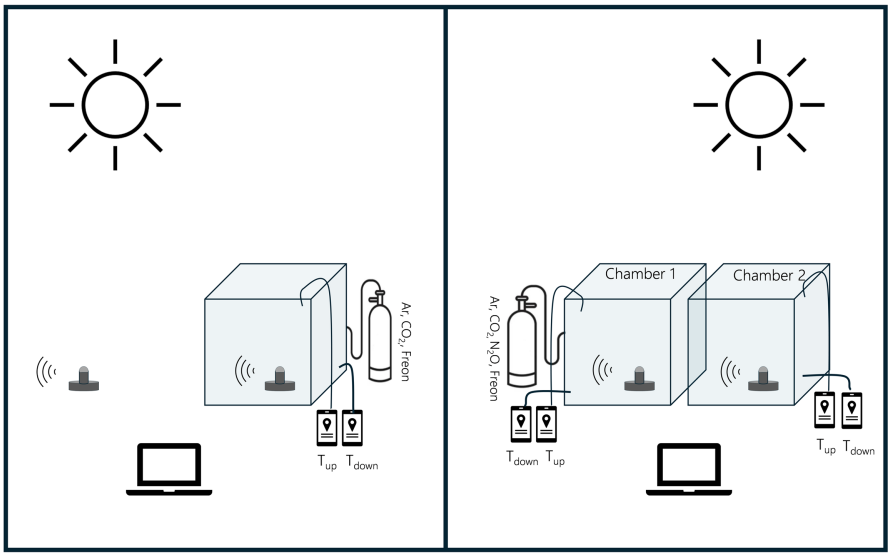

Figure 8. The left side illustrates the mobile measurement setup used in the White Desert in Egypt, while the right side represents the stationary setup applied in Vienna. Both used thin PE-foiled cuboid skeletons to prevent major gas loss.

For each setup we used two identical SL-510 Upward-Looking apogee pyrgeometers (see Figure 9) for longwave radiation measurement.

Elitech GSP-6 temperature and humidity dataloggers were placed at close to the bottom and at the top of the test chambers to provide vertical profiling. We used a low-cost UT A37 CO_2 NDIR sensor and portable analyzer GA-S1 for O_2 and CO_2 with measurement ranges of 0% - 1% and 0% - 25 % respectively. Furthermore, we used controlled concentrations of CO_2, Ar, N_2O (nitrous oxide) and Freon R-134a, where the latter two are known as strong greenhouse gases. The thermal status of the setups was checked via a HX1 Infrared-Thermogra-

phy-Camera.

Figure 9. Apogee SL-510 upward-looking pyrgeometer with Bluetooth microcache datalog-ger.

Figure 10 was obtained by a comparative measurement at the Vienna location at clear sky conditions. The results showed that the systematic error between both units and therefore also the differential resolution limit is 0.5 W/m^2.

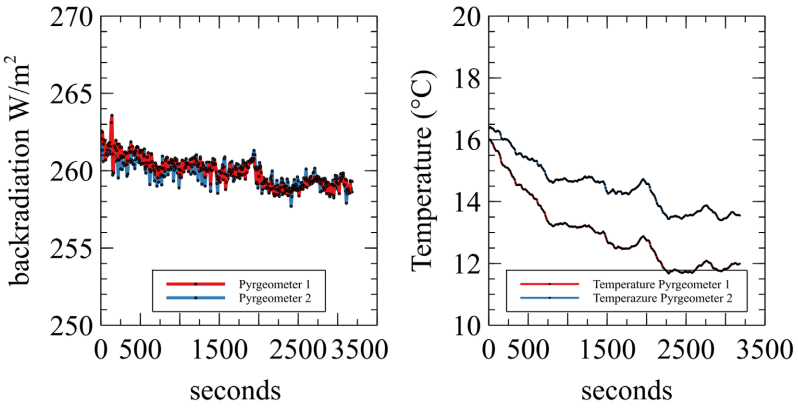

Figure 10. Pyrgeometers 1 and 2 compared to each other at clear skies at the Vienna location.

2.3. Analytical Methods

The publicly available version of MODTRAN [13], provided by the University of Chicago, allows us to specify the altitude at which the longwave radiation is measured and the direction from which it is detected. Usually, it is applied for choosing a virtual position at a certain altitude, for example 70 km, to measure the upwelling long-wave radiation. The portion that does not arrive is absorbed in the atmosphere. This measurement provides information about how much radiation the Earth ultimately emits into space—or vice versa how much is lost in the atmosphere and mainly back radiated to the surface.

This tool can therefore be used for estimating the order of magnitude of back

radiation increase (see Figure 11) within the respective test-chambers due to the higher greenhouse gas concentrations and applying a virtual 0.5% humidity increase to simulate the effect of a 10 µm transparent PE foil.

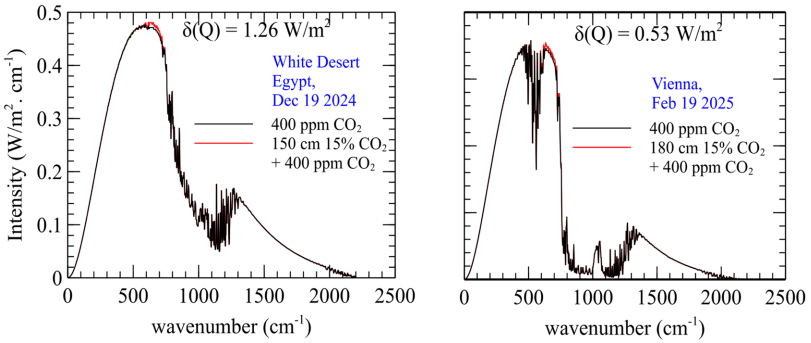

Figure 11. The left shows the MODTRAN simulated back radiation at the White Desert location when adding 150 cm column of 15 vol% CO_2, while the right side shows the MODTRAN simulated back radiation at the Vienna location adding 180 cm of 15 vol% CO_2.

The difference in simulated back radiation between the two locations is primarily attributed to the varying levels of solar irradiance at the surface (LAT 48˚ vs. 27˚), which becomes particularly relevant given the differential resolution limit of 0.5 W/m² of our instruments. Higher solar irradiance can lead to greater surface heating and thus potentially influence the overall radiative balance.

3. Results

3.1. Infrared Back Radiation Distribution

Measurements were carried out at two field sites: the White Desert in Egypt and the Vienna region. To reduce potential data degradation caused by environmental influences—particularly wind-induced disturbances—measurements at both locations were conducted under conditions of relatively low wind speeds, which are especially difficult to achieve during the winter months. The implemented experimental setups (Figure 12) correspond to the schematic representations provided earlier (Figure 8).

Figure 12. Illustrations of Figure 8 were applied at the White Desert location in Egypt and at the Vienna area location. To prevent too strong deteriorations of our measurements it was necessary in both cases to use positions at relatively low wind conditions, which is difficult during wintertime.

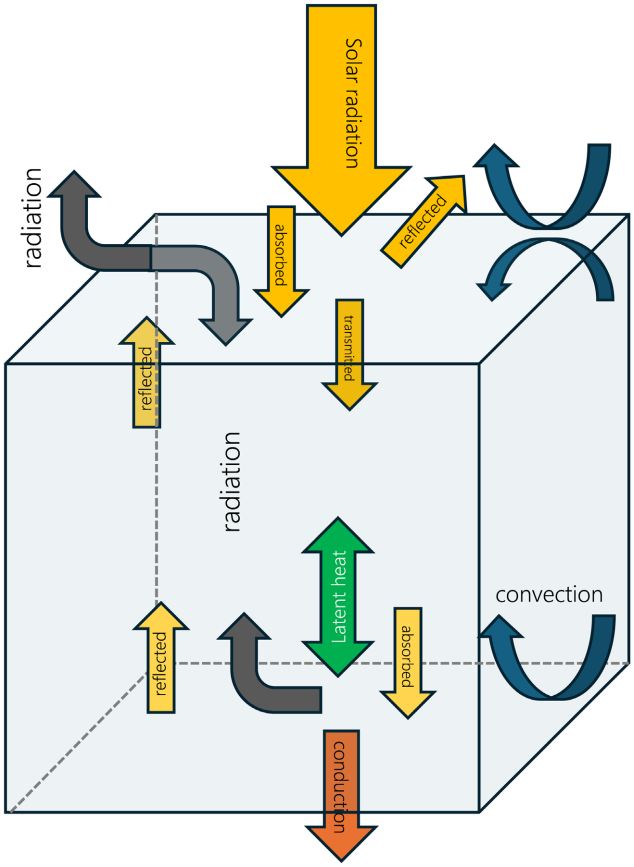

Figure 13. Schematic representation of greenhouse climate model flows related to convection, conduction, short-wave radiation and long-wave radiation.

Above schematics (**Figure 13**) are similar to the modeling of greenhouses for plant growth [16] and adopt pyrgeometer calibration in a housed setup with a modified 3-coefficients model [17] [18]:

$$W_{in} = K_1 V_{tp} + K_2 \sigma T_{\text{case}}^4 + K_3 \sigma \left(T_{\text{dome}}^4 - T_{\text{case}}^4 \right) \tag{1}$$

with K_i as pyrgeometer calibration coefficients and V_{tp} as thermopile output voltage, T_{case} the instrument case temperatures, T_{dome} the interference filter temperature and the incoming longwave irradiance W_{in}.

When considering the left scenario of **Figure 8** used in the White Desert and using above model we can describe the measured downwelling heat radiation flux Q_2 in the test chamber by

$$Q_2(t) = a_1 \left(T_2(t) - T_1(t) \right) + a_2 L\left(T_2(t) \right) + b_1 T_1(t)^4 + b_2 T_2(t)^4 + c_1 Q_1(t) + \delta Q \tag{2}$$

with $T_2 = T_{\text{case}}$, $T_1 = T_{\text{dome}}$, $Q_2 \approx W_{in}$, $c_1 Q_1 \approx K_1 V_{tp} + K_2 \sigma T_{\text{case}}^4$,

$$b_1 T_1(t)^4 + b_2 T_2(t)^4 \approx K_3 \sigma \left(T_{\text{dome}}^4 - T_{\text{case}}^4 \right), \quad a_1 \left(T_2(t) - T_1(t) \right) + a_2$$

convection and $a_2 L\left(T_2(t) \right)$ latent heat. The latent heat is given by a polynomial expression [19]

$$L(T) = L_{\text{water}}(T) \approx \left(2500.8 - 2.36T + 0.0016T^2 - 0.00006T^3 \right) \text{J/g} \tag{3}$$

and δQ is the excess radiation flow from increased greenhouse gas back radiation, determined by least square fitting using equation (2) and calibration of the parameters to pure air filling, with

a_1	−7.39	W/(m²K)
a_2	4.54E−02	W/(m²g/J)
b_1	−6.81E−08	W/(m²K⁴)
b_2	6.83E−08	W/(m²K⁴)
c_1	7.63E−01	

Using 15 vol% CO_2, 15% Ar and less than 1% R134a tetrafluoroethane freon fillings we obtained (as can be seen from Figure 14)

Test gas	CO_2	Ar	RS134a
δQ (W/m²)	1.5	0	15

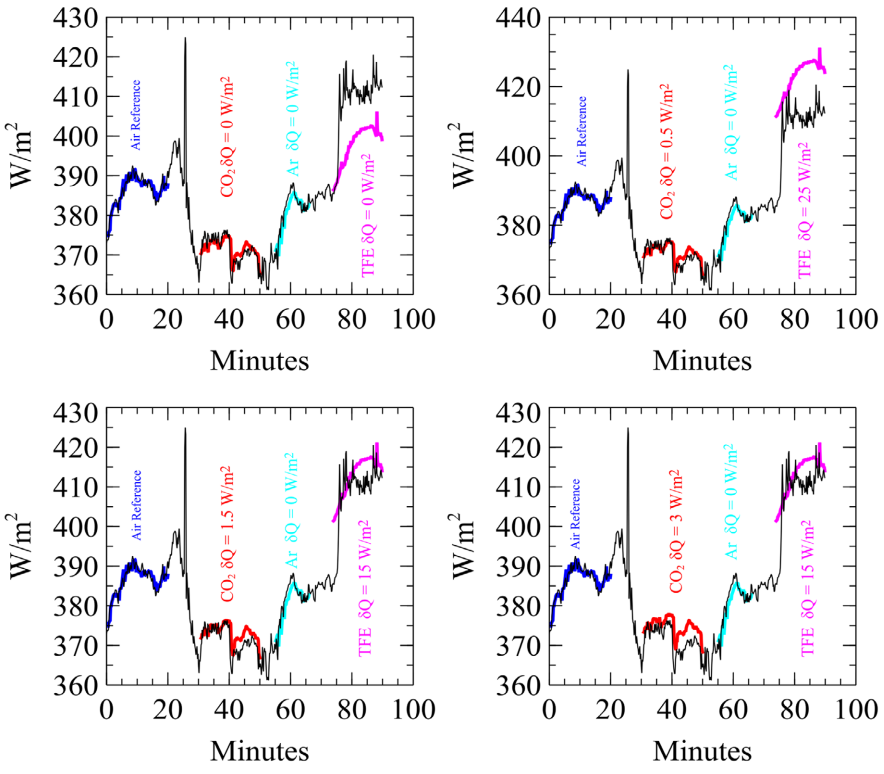

Figure 14. Results of measurements in the Egyptian White Desert using the setup of Figure 8 at various values of backradiation differences to a pure 400 ppm vol CO_2 air column.

A purely graphical evaluation of the raw data by subtracting the pyrgeometer data inside and outside the foiled greenhouse (Figure 15 left side) shows a somewhat stronger increase in back radiation at 15 vol% CO_2 of 2.1 W/m², due to the

systematic measurement errors between both sensors of 0.5 W/m² and obvious differences in the actual weather conditions compared to the ideal MODTRAN scenarios.

The red solar baseline represents the additional mean IR radiation from the PE film obtained through the Loess filter due to the changing position of the sun. The right figure shows the additional back radiation by using IR active gases in such a field test chamber at the White Desert location. Fluctuations and some large peaks are related to handling and manipulation of gas supplies and other units, but also due to variations in the cloud coverage and wind gusts at the time of IR data acquisition.

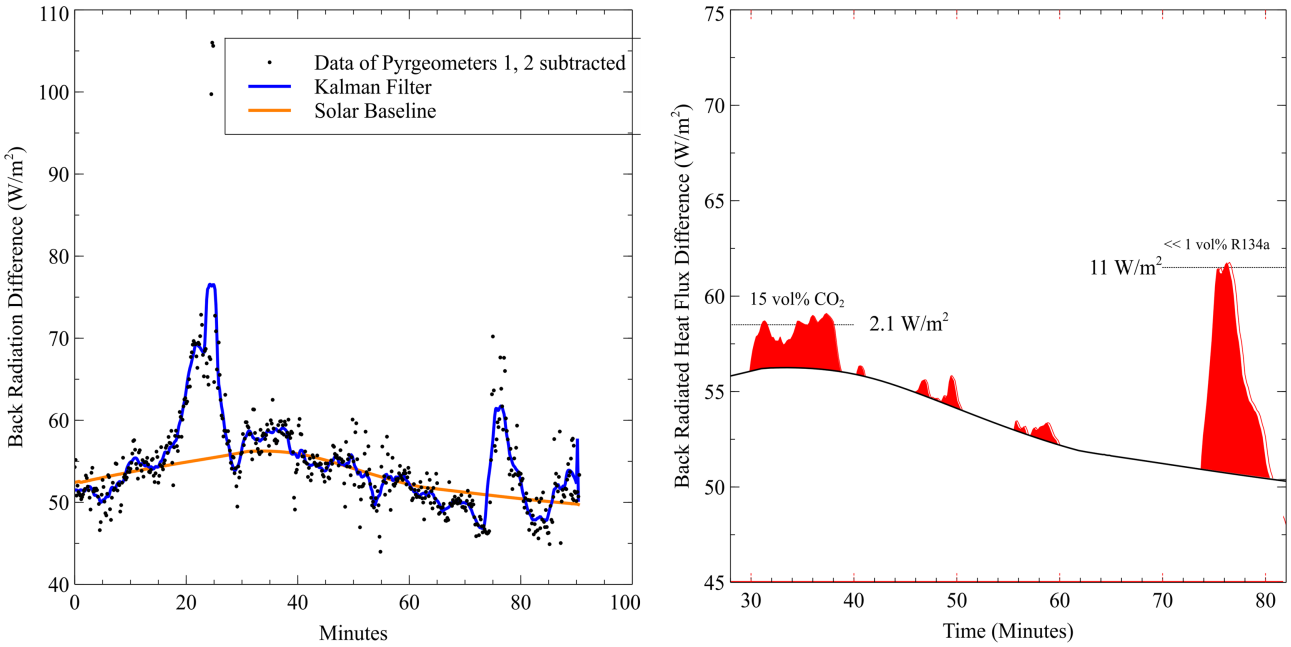

Figure 15. Results of measurements in the Egyptian White Desert using the setup of **Figure 8** and subtracting the back radiation data unhoused pyrgeometer from the test chamber housed twin. Data smoothing used a Kalman filter and background trend is summarized by the solar baseline expressing changing solar irradiance on the protective foil dome.

The rather difficult desert conditions only allowed for one measurement run and encouraged further field tests at more favorable conditions at another location, even at lower solar irradiation conditions.

Discrepancies between the model-derived CO_2 impact and graphical evaluation suggests potential inaccuracies in the used model, but due to the small nature of the IRBR in this concentration regimes field measurements always will suffer under various transient environmental conditions and should be treated statistically. We doubt that other complex feedback play a significant role in the results, as the system response is synchronous to the parameter variation.

Measurements in the Vienna area were conducted under dry and clear sky conditions on February 19 and 20 of this year. Air temperature (**Figure 16**), humidity (**Figure 17**), and global radiation (**Figure 18**) data were obtained from the official weather station of the University of Natural Resources and Life Sciences, Vienna.

As laid out before two gas chambers with the same dimensions (L = 100 cm, W = 62 cm, H = 184 cm) and enclosed with PE foil were positioned 5 cm apart (Figure 8). Each gas chamber was equipped with a centrally aligned pyrgeometer. D2 placed in the air-filled reference chamber, while pyrgeometer D1 was used in the chamber filled with test gases. The raw data shows thermal stabilization up to minute 40 (Figure 20), high fluctuations in the back radiation due to adjustment and preparatory work, and the repeated CO_2 filling from minute 40 onwards (Figure 19). Thus, three runs with CO_2 inflow were carried out up to minute 125, whereby the slight fluctuations and decreases in concentrations after the interruption of the CO_2 gas flow can be explained by the leak rate due to leaks in the foil skin.

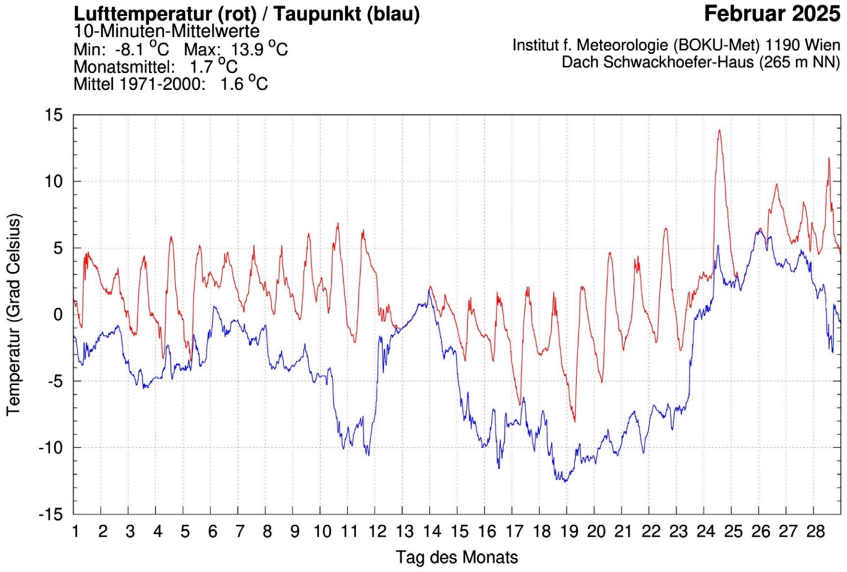

Figure 16. Air temperature vs. dew point temperature in the month of February 2025 for Vienna [20].

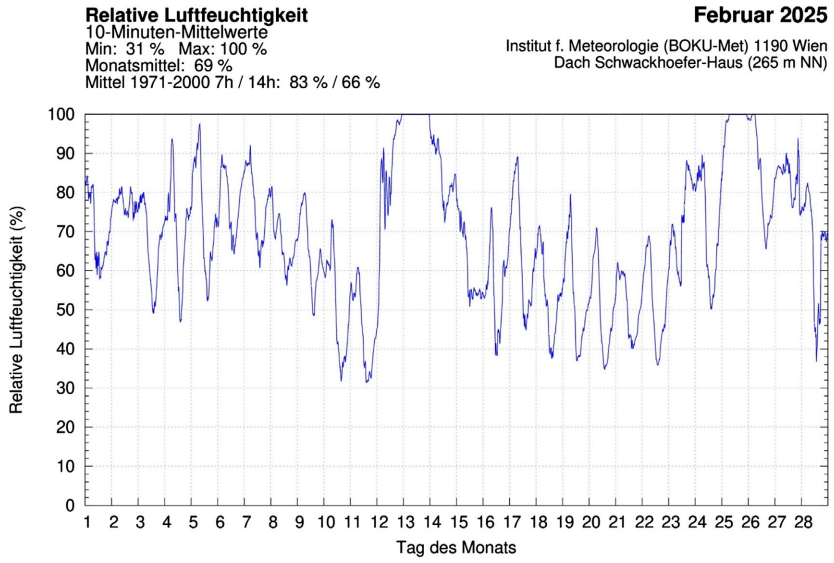

Figure 17. Relative humidity in the month of February 2025 for Vienna [20].

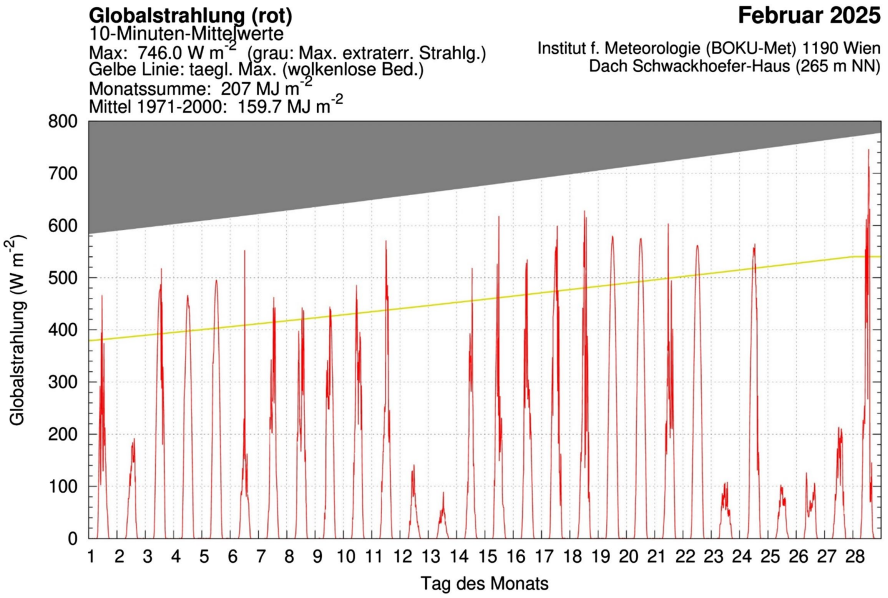

Figure 18. Global solar irradiation in the month of February 2025 for Vienna [20].

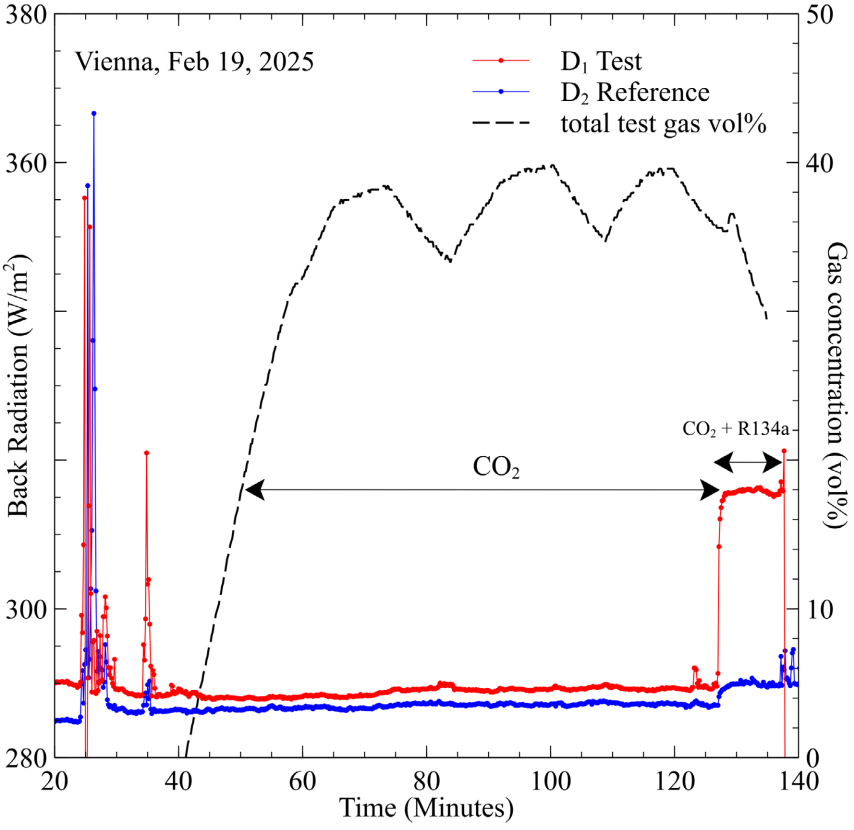

Figure 19. Raw data obtained on Feb 19 by the two pyrgeometers in test chamber 2 and reference chamber 1 at variable gas concentrations of CO_2 and R134a Freon-CO_2.

As we used a Bluetooth regulated low power ventilator to artificially force convection in chamber 1 it is no surprise that the temperature profiles in this chamber are not so spread in magnitude as in chamber 2.

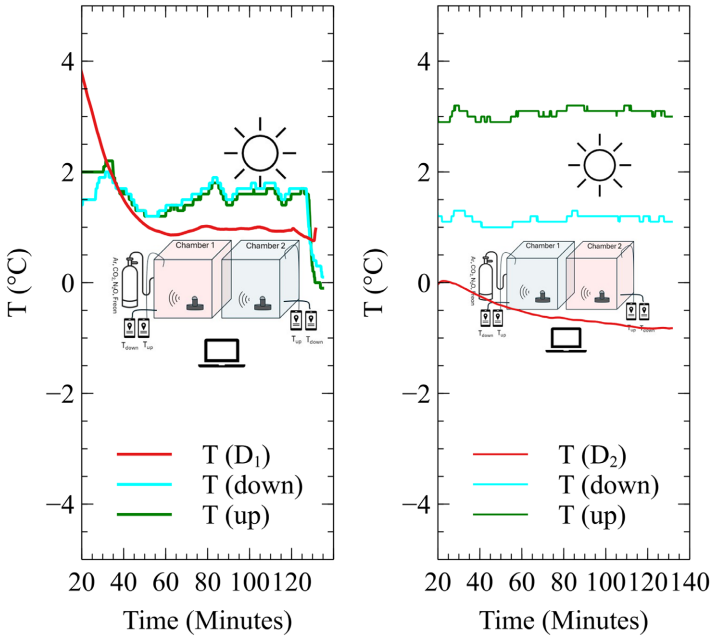

Figure 20. Temperature data obtained on Feb 19 by various thermoelements in test chamber 2 and reference chamber 1 at variable gas concentrations of CO_2 and R134a Freon.

In general, despite the increase in CO_2 concentration from 0.04% (normal atmospheric CO_2 concentration) to an average of 40% within chamber 1, there is hardly any increase in backscattering, which in turn confirms the near saturation of IR backscattering by the CO_2 already present in the atmosphere in the ppm regime, which was also the goal of our measurements. Of course, these statements refer to a 180 cm high column of air but can be converted accordingly to the entire atmosphere in the ppm scale using the MODTRAN simulation, which provided indeed the correct order of magnitude estimation of the measured increase.

Starting at minute 127, the potent greenhouse gas Freon RS134a was introduced in relatively small quantities, leading to a sharp increase in infrared backscattering (**Figure 19**). This gas does not occur naturally and is also associated with the destruction of the UV-protective stratospheric ozone. This strong IR radiation from the test chamber could also be observed experimentally with detector D2 in the reference chamber by crosstalk, as the 10 µm-thick foils only partially absorb the IR radiation and can even be used as a kind of low-pass filter to eliminate transient interference.

Increasing the Ar concentration from 0.934% (normal atmospheric Ar concentration) to an average of 40% within chamber 1, there is no response in the back radiation, which is of course not surprising for a non-IR active noble gas, serving simply as a reference. Feeding a limited amount of N_2O into the Ar-enriched test chamber proves the IR reactivity of a stronger greenhouse gas, while diluting it with CO_2 reduces the back radiation back to atmospheric levels. This is another proof of the small to vanishing effect of additional CO_2 in the test chamber and in the ppm regime of the atmosphere.

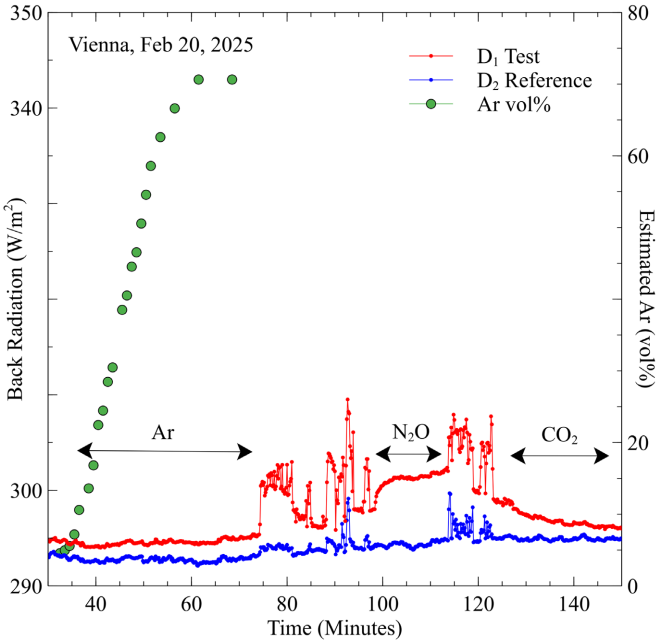

Figure 21. Raw data obtained on Feb 20 by the two pyrgeometers in test chamber 2 and reference chamber 1 at variable gas concentrations of Ar and N_2O and CO_2.

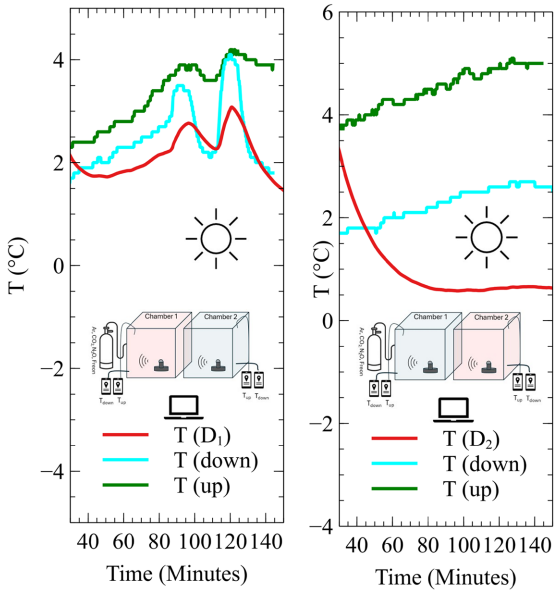

Figure 22. Temperature data obtained on Feb 20 by various thermoelements in test chamber 2 and reference chamber 1 at variable gas concentrations of Ar and N_2O-Ar and CO_2-N_2O-Ar.

The artificially forced convection in chamber 1 shows again less temperature spreading of the measured temperatures than reference chamber 2 without forced convection (**Figure 22**). We clearly observe that the Joule Thompson effect of Ar is small to negligible compared to the Joule Thompson effect of R134a, N_2O and CO_2, corresponding to their respective specific heat capacity cp. (Note: by expanding the gases into test chamber 1, this Joule Thomson effect is temporary visible).

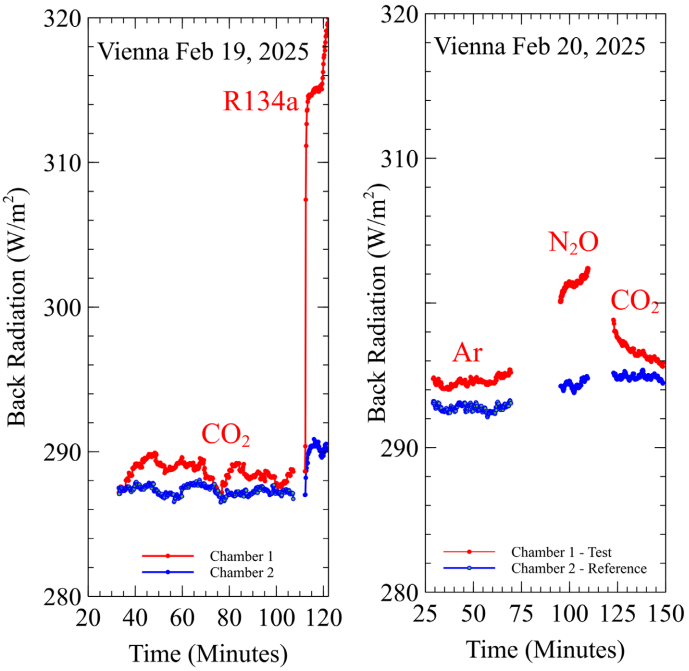

Figure 23. Backscattered infrared radiation data recorded on February 19 and 20, following the exclusion of artifacts introduced by handling and experimental manipulations.

These measurements of backscattering (**Figure 23**) by increasing the CO_2 concentration are graphically indistinguishable from the simulation results with MODTRAN. The logarithmic increases are also compatible with each other at 6.4 (MODTRAN) and 6.76 (this measurement) (**Figure 24**).

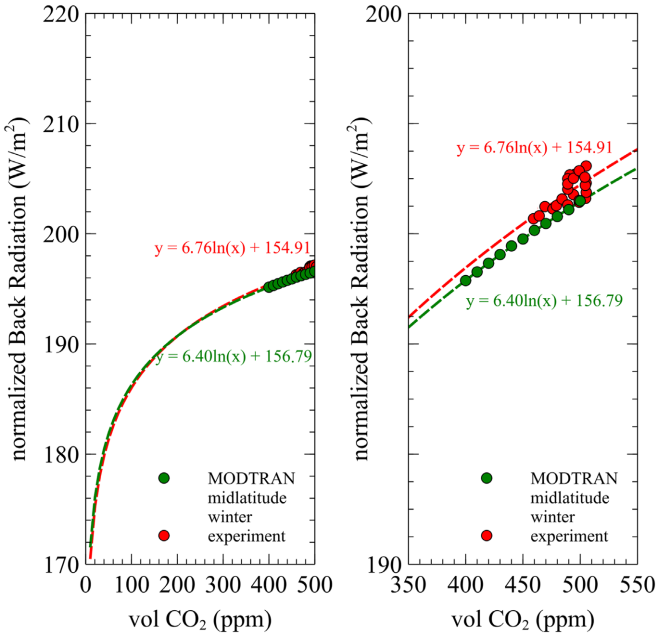

Figure 24. Test chamber CO_2 concentrations converted into atmospheric column concentrations vs. normalized Back Radiation data from **Figure 19** compared to MODTRAN simulations at Midlatitude winter.

On Feb 20, we used Argon gas to dilute the natural CO_2 concentration in the test chamber and found that the logarithmic radiation decrease (**Figure 25**) behaves very similar to the increase shown in **Figure 24**.

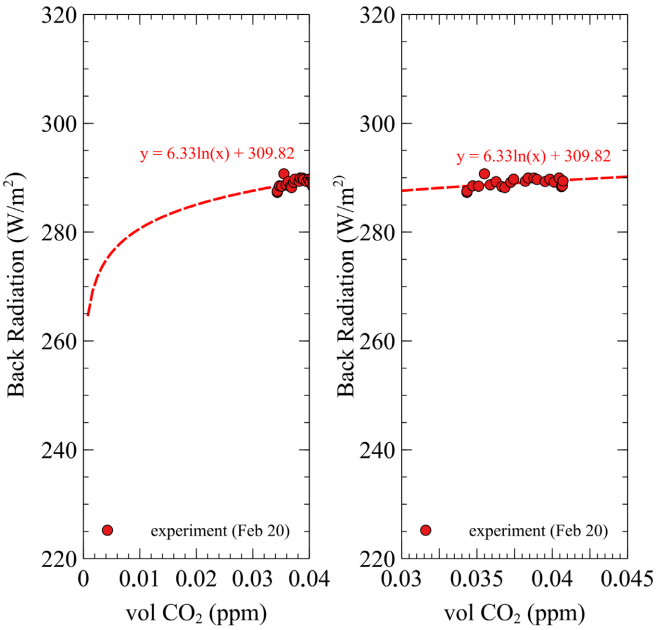

Figure 25. Test chamber CO_2 concentrations during Argon flooding converted into atmospheric column concentrations vs. normalized Back Radiation data from **Figure 21**.

In summary, it can be said that increasing the CO_2 concentration hardly leads to an increase in infrared backscattering, whereas even comparably small values of RS134a lead to a massive response. The logarithmic law of radiative forcing coincides well with MODTRAN calculations. This proves that MODTRAN in fact is a practical tool to predict climate forcing due to CO_2 increases on a global scale.

The right curve in **Figure 26** uses the usual IPPC AR6 featured [30] modified Planck climate-sensitivity with $\lambda_0 = 0.31\,\mathrm{K}\cdot\mathrm{W}^{-1}\cdot\mathrm{m}^2$ to obtain the expected zero-feedback temperature changes from CO_2 forcing alone. Without having a clear and unambiguous model and experimental setup all feedback multiplicators are highly speculative and outside statistical confidence. In future work we will refer to this problem to support attempts for more transparency on this issue.

3.2. Factors Affecting Infrared Backradiation

Infrared backradiation (IRBR) is a critical component of the Earth's energy balance, representing the longwave radiation emitted by the atmosphere back towards the surface. IRBR is fundamentally a function of surface temperature, , the amount of IR-active gases and various atmospheric conditions such as humidity and cloud coverage. To minimize the influence of the latter two forcings in our study, we strategically chose to conduct measurements under appropriate desert and winter conditions, characterized by low humidity and minimal cloud cover.

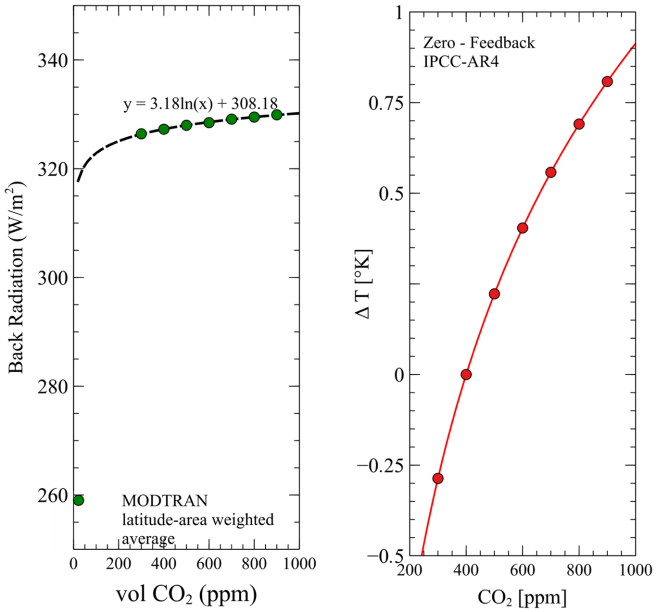

Figure 26. Using MODTRAN at all available clear sky scenarios, averaging them latitude area weighted and temperature changes as resulting from Stephan-Boltzmann radiation law.

3.2.1. Greenhouse Gas Concentrations

The abundance of greenhouse gases (GHGs) in the atmosphere is the primary driver of IRBR. Gases like water vapor (H_2O), carbon dioxide (CO_2), methane (CH_4), nitrous oxide (N_2O), ozone (O_3), and various halocarbons absorb outgoing longwave radiation emitted by the Earth's surface at specific wavelengths. These absorbed photons are then re-emitted in all directions, with a significant portion directed back towards the surface, contributing to the warming of the lower atmosphere and the surface—the greenhouse effect [21]. The strength of this effect for each gas depends on its concentration, its radiative efficiency (how much energy it absorbs and re-emits per molecule), and the wavelengths at which it absorbs. For instance, water vapor, with its high atmospheric variability, is the most potent absorber across a broad spectrum of infrared wavelengths, playing a dominant role in the natural greenhouse effect [22] [23]. Carbon dioxide, while having specific absorption bands, contributes much less than water vapor due to its natural atmospheric concentrations and to a lower degree from anthropogenic activities [24]. In addition, the narrow absorption bands of CO_2 overlap with the absorption bands of water vapor. The concept of radiative forcing quantifies the change in the Earth's energy balance due to alterations in GHG concentrations or other factors.

3.2.2. Cloud Cover and Atmospheric Variability

Clouds exert a significant and multifaceted influence on IRBR through their ability to absorb and emit longwave radiation [25]. The net radiative effect of clouds depends on their type, altitude, thickness, and temperature. Low-level clouds, with temperatures closer to the surface, emit a substantial amount of infrared radiation downwards, enhancing IRBR [26]. High-level, colder clouds, like cirrus, emit less

downward longwave radiation but can be more transparent to outgoing longwave radiation, potentially leading to a net cooling effect in some cases, although their thin ice crystal structure can also contribute to trapping outgoing radiation. The fractional coverage of clouds, their optical properties (related to their liquid water or ice content and droplet/crystal size), and their vertical distribution are crucial parameters in determining their overall impact on IRBR and the Earth's radiative balance. Varying cloud covers and wind speeds are clearly visible in the obtained data. In our study, the contributions of these fluctuating atmospheric conditions were minimized by employing differential methods using two identical pyrgeometers positioned side by side, allowing for the cancellation of common-mode variations.

3.2.3. Atmospheric Temperature Profile

The vertical distribution of temperature in the atmosphere directly affects the emission of infrared radiation according to the Stefan-Boltzmann law. Warmer atmospheric layers emit more longwave radiation. The temperature profile is influenced by various processes, including the absorption of solar radiation by the surface and atmosphere, the release of latent heat during condensation, and the dynamical transport of heat through atmospheric circulation [27]. Changes in the atmospheric temperature profile, often driven by alterations in GHG concentrations and radiative forcing, can lead to significant changes in the magnitude and spectral distribution of IRBR reaching the surface. For example, a warmer lower troposphere, resulting from increased greenhouse gas concentrations, will emit more infrared radiation downwards.

3.2.4. Surface Properties

While the Earth's surface is the primary emitter of outgoing longwave radiation, its properties indirectly influence IRBR by determining the characteristics of the radiation available for atmospheric absorption and re-emission. The surface temperature T_s determined by the balance of incoming solar and longwave radiation and outgoing longwave, sensible, and latent heat fluxes, dictates the initial amount of longwave radiation emitted upwards $L_{up} = \varepsilon_s \sigma T_s^4$ where ε_s is surface emissivity and σ is the Stefan-Boltzmann constant. Surface emissivity ε_s, which varies with surface type (e.g., desert sand, vegetation, water) and wavelength, affects the efficiency of this emission [28]. Differences in surface albedo also play a crucial role by influencing the amount of solar radiation absorbed by the surface, thereby affecting surface temperature and subsequent longwave emission.

3.2.5. Atmospheric Aerosols

Atmospheric aerosols, tiny solid or liquid particles suspended in the air, can also interact with longwave radiation through absorption and emission. The magnitude and sign of their radiative forcing in the infrared spectrum depend on their composition, size, shape, and vertical distribution. For instance, dust aerosols, common in desert regions, can absorb and emit infrared radiation, potentially af-

fecting local IRBR. While their direct impact on IRBR is generally considered smaller compared to GHGs and clouds on a global scale, in specific environments or during significant aerosol events (e.g., volcanic eruptions, dust storms), their contribution can be non-negligible. Furthermore, aerosols play a critical indirect role by acting as cloud condensation nuclei and ice nuclei, thereby influencing cloud formation and properties, which in turn significantly affect IRBR.

3.2.6. Experimental Considerations with Test Chamber

In addition to the natural atmospheric factors, the methodology employed in studying IRBR can introduce its own influences. Using a foiled test chamber for studying concentration-dependent IR effects implies also dealing with a 1.5 - 3 W/m^2 additional IR radiation from the differences in PE foil thickness warming up from long- and shortwave irradiation. However, this difference was reduced to negligible magnitudes by temperature calibration of the pyrgeometers. This highlights the importance of carefully accounting for the radiative properties of experimental setups when conducting such investigations.

3.2.7. Atmospheric Composition (Beyond Major GHGs)

Besides the primary greenhouse gases that constitute a significant portion of the atmosphere, trace gases and variations in the overall atmospheric composition can exert a considerable influence on IRBR. Some trace gases, even at very low concentrations (parts per billion or even trillion), possess strong absorption bands in the infrared spectrum, leading to a disproportionately large radiative forcing per molecule. Halogenated gases, such as the R-134a investigated in our study, are prime examples of such potent greenhouse gases [29]. Changes in the concentrations of these radiatively active trace gases, often due to industrial emissions, can contribute significantly to alterations in IRBR and the overall energy balance of the Earth's system. Furthermore, the presence of other atmospheric constituents, even those not classified as GHGs (like Argon as investigated in our study), can have subtle influences on the spectral properties of atmospheric transmission and emission.

Understanding the relative contributions and complex interactions of these factors is essential for accurately interpreting measurements of IRBR and for developing reliable climate models that can project future climate change. Our study focuses on isolating the impact of specific greenhouse gases on IRBR in the unique context of a desert environment and cold cloudless winter days at mid-latitudes, where the influence of factors like water vapor and cloud cover is often minimized, allowing for a clearer investigation of the radiative properties of other atmospheric constituents.

4. Discussion

The findings of this study, conducted under the unique conditions of the White Desert in Egypt and compared with measurements in Vienna, provide valuable insights into the radiative impact of greenhouse gases on infrared back radiation

(IRBR), particularly in arid environments. Our MODTRAN simulations and field measurements suggest a limited additional impact on IRBR even at strongly elevated concentrations of CO_2, which aligns with the concept of saturation in its radiative forcing capacity at higher concentrations. This observation, while seemingly counterintuitive given the ongoing increase in atmospheric CO_2, underscores the complex interplay of radiative transfer in the atmosphere and the limitations in IRBR enhancement at very high local CO_2 levels very clear. The study focused on short-term measurement campaigns, not capturing long-term variability in IRBR dynamics and therefore only on time synchronous IRBR response to gas parameter variations. Most reliable and proven radiation models, like MODTRAN, provide only these results and so we focused here on testing their predictions.

In contrast, the disproportionately high radiative forcing observed with the introduction of R-134a, even at trace concentrations, highlights the significant impact of potent synthetic greenhouse gases on the Earth's energy balance. This finding reinforces the concerns regarding the use and release of such gases, as their radiative efficiency far exceeds that of CO_2 on a per-molecule basis. The experimental observation of a substantial increase in IRBR within the test chamber upon the introduction of R-134a, even detectable by the pyrgeometer in the adjacent reference chamber, underscores the potency of these gases in altering radiative fluxes. This finding has significant implications for more realistic climate mitigation strategies, emphasizing the need to control and phase out high-GWP (Global Warming Potential) substances like R-134a.

The comparison between the desert and Vienna datasets offers further context. The lower initial IRBR in the dry, clear atmosphere of the White Desert, coupled with high solar irradiance, provided a distinct backdrop for observing changes due to increased GHG concentrations. The somewhat more humid but clear sky conditions in Vienna helped further to isolate IRBR changes induced by CO_2 within our chosen experimental setup. The challenges encountered during the desert measurements, including the limited experimental time window at unexpected fluctuating weather conditions, highlight the difficulties of conducting more precise radiative measurements in extreme environments. The more root-controlled conditions in Vienna allowed also for longer experimental time windows, but further emphasizing the need for well-controlled experiments to isolate the effects of individual greenhouse gases.

Our attempt to simulate the effect of the PE foil using a virtual increase in relative humidity in MODTRAN is a simplification and warrants further investigation. The distinct IR absorption spectra of water vapor and polyethylene likely introduce some degree of uncertainty in our simulations.

Future studies could benefit from more sophisticated modeling approaches that explicitly account for the radiative properties of the enclosure material.

The energy balance fit model (equ. 2) provided a quantitative approach to estimate the excess radiation flow δQ resulting from increased greenhouse gas concentrations. The derived values, while showing a limited impact for CO_2 and a

substantial impact for R-134a, are subject to the accuracy of the model parameters and the inherent complexities of the experimental setup. The discrepancy between the model-derived CO_2 impact and the purely graphical evaluation suggests the need for further refinement of the model and more extensive datasets.

5. Conclusions

This study provides empirical evidence of the differential radiative impact of greenhouse gases on infrared back radiation under contrasting environmental conditions. IRBR saturation behavior for increasing CO_2 well above 400 ppm under laboratory conditions was described in our last study [30] and now confirmed by these findings under natural conditions in the field. While increasing CO_2 concentrations may therefore have a limited additional effect on IRBR, potent synthetic gases like R-134a exert a disproportionately strong radiative forcing. This highlights the critical importance of focusing on the mitigation of these high-GWP (greenhouse warming potential) gases—instead of focusing on CO_2 reduction which effect in increasing IRBR is already largely saturated in earth atmosphere within the orders of magnitude of the anthropogenic emission potential—to effectively address climate change.

The extreme conditions of the White Desert, characterized by low humidity and high solar radiation, offer a unique natural laboratory for studying radiative processes. However, conducting precise measurements in such environments presents significant challenges. The comparative measurements in Vienna, under more stable conditions, provided valuable complementary data.

Future research should focus on:

- Conducting longer-duration measurements under controlled conditions to improve the robustness of the results.
- Employing more sophisticated radiative transfer models that account for the specific properties of experimental enclosures.
- Investigating the synergistic effects of different greenhouse gases on IRBR in various climatic regimes.
- Expanding the study to include a wider range of trace gases known to have significant radiative forcing potential.

Ultimately, a more comprehensive understanding of the radiative impacts of various greenhouse gases in different environments is crucial for refining climate models and developing effective strategies to mitigate a possible anthropogenic climate change, particularly in vulnerable arid regions.

Conflicts of Interest

The authors declare no conflicts of interest regarding the publication of this paper.

References

[1] Li, X., Xu, H. and Yang, K. (2013) The Impact of Infrared Back-Radiation on the Surface Energy Balance in Deserts. *Geophysical Research Letters*, **40**, 2405-2410.

[2] Boucher, O. and Reddy, M.S. (2008) Global Climate Change: Implications for the Energy Balance. *Nature Geoscience*, **1**, 713-718.

[3] Fisher, R.A. and Knutti, R. (2015) The Influence of Surface Properties and Radiative Fluxes on Climate Sensitivity. *Nature Climate Change*, **5**, 3-6.

[4] Ramanathan, V. and Feng, Y. (2009) Air Pollution, Climate Change, and Global Warming: Global and Regional Perspectives. *Atmospheric Environment*, **43**, 37-41.

[5] Charney, J.G. and Shukla, J. (1981) The Role of Desertification in the Global Climate System. *Science*, **213**, 979-988.

[6] Stephens, G.L. (2005) Cloud Feedbacks in the Climate System: A Critical Review. *Journal of Climate*, **18**, 237-273. https://doi.org/10.1175/jcli-3243.1

[7] Wielicki, B.A., Barkstrom, B.R., Harrison, E.F., Lee, R.B., Louis Smith, G. and Cooper, J.E. (1996) Clouds and the Earth's Radiant Energy System (CERES): An Earth Observing System Experiment. *Bulletin of the American Meteorological Society*, **77**, 853-868. https://doi.org/10.1175/1520-0477(1996)077<0853:catere>2.0.co;2

[8] Loeb, N.G., *et al*. (2009) Toward a More Accurate Description of Earth's Energy Budget: The CERES Mission. *Bulletin of the American Meteorological Society*, **90**, 611-624.

[9] Loeb, N.G., Doelling, D.R., Wang, H., Su, W., Nguyen, C., Corbett, J.G., *et al*. (2018) Clouds and the Earth's Radiant Energy System (CERES) Energy Balanced and Filled (EBAF) Top-of-Atmosphere (TOA) Edition-4.0 Data Product. *Journal of Climate*, **31**, 895-918. https://doi.org/10.1175/jcli-d-17-0208.1

[10] Salisbury, J.W. and D'Aria, D.M. (1992) Emissivity of Terrestrial Materials in the 8-14 μm Atmospheric Window. *Remote Sensing of Environment*, **42**, 83-106. https://doi.org/10.1016/0034-4257(92)90092-x

[11] Hanel, R.A. and Conrath, B.J. (1970) Thermal Emission Spectra of the Earth and Atmosphere from the Nimbus 4 Michelson Interferometer Experiment. *Nature*, **228**, 143-145. https://doi.org/10.1038/228143a0

[12] Zhou, L. (2016) Desert Amplification in a Warming Climate. *Scientific Reports*, **6**, Article No. 31065. https://doi.org/10.1038/srep31065

[13] MODTRAN Infrared Light in the Atmosphere. https://climatemodels.uchicago.edu/modtran/modtran.doc.html

[14] Zhou, C. and Wang, K. (2016) Land Surface Temperature over Global Deserts: Means, Variability, and Trends. *Journal of Geophysical Research*: *Atmospheres*, **121**, 14,344-14,357. https://doi.org/10.1002/2016jd025410

[15] Ogawa, K. and Schmugge, T. (2004) Mapping Surface Broadband Emissivity of the Sahara Desert Using ASTER and MODIS Data. *Earth Interactions*, **8**, 1-14. https://doi.org/10.1175/1087-3562(2004)008<0001:msbeot>2.0.co;2

[16] Halling, M. (2024) Greenhouse Energy Balance: A Numerical Approach to Analyze the Influence of Location, Season, and Structural Design of Greenhouses. https://liu.diva-portal.org/smash/get/diva2:1885951/FULLTEXT01.pdf

[17] Stoffel, T., *et al*. (2006) Pyrgeometer Calibrations for the Atmospheric Radiation Measurement Program: Updated Approach. *Extended Abstracts*, 16*th ARM Science Team Meeting*, Albuquerque, 27-31March 2006, 1-18.

[18] Philipona, R., Dutton, E.G., Stoffel, T., Michalsky, J., Reda, I., Stifter, A., *et al*. (2001) Atmospheric Longwave Irradiance Uncertainty: Pyrgeometers Compared to an Absolute Sky-Scanning Radiometer, Atmospheric Emitted Radiance Interferometer, and Radiative Transfer Model Calculations. *Journal of Geophysical Research*: *Atmospheres*, **106**, 28129-28141. https://doi.org/10.1029/2000jd000196

[19] Rogers, R.R. and Yau, M.K. (1989) A Short Course in Cloud Physics. 3rd Edition, Pergamon Press, 16.

[20] Monatsübersicht Wetterstation BOKU-Met Februar 2025. https://meteo.boku.ac.at/wetter/mon-archiv/2025/202502/202502.html

[21] IPCC (2021) Climate Change 2021: The Physical Science Basis. Contribution of Working Group I to the Sixth Assessment Report of the Intergovernmental Panel on Climate Change. Cambridge University Press. https://doi.org/10.1017/9781009157896.001

[22] Soden, B.J. and Held, I.M. (2006) An Assessment of Climate Feedbacks in Coupled Ocean-Atmosphere Models. *Journal of Climate*, **19**, 3354-3360. https://doi.org/10.1175/jcli3799.1

[23] Pierrehumbert, R.T. (2010) Principles of Planetary Climate. Cambridge University Press. https://doi.org/10.1017/cbo9780511780783

[24] Hartmann, D.L. (1994) Global Physical Climatology. Academic Press.

[25] Wallace, J.M. and Hobbs, P.V. (2006) Atmospheric Science: An Introductory Survey. Academic Press.

[26] Forster, P., *et al*. (2007) Changes in Atmospheric Constituents and in Radiative Forcing. In: *Climate Change* 2007: *The Physical Science Basis*. *Contribution of Working Group I to the Fourth Assessment Report of the Intergovernmental Panel on Climate Change*, Cambridge University Press, 129-234.

[27] Liou, K.N. (2002) An Introduction to Atmospheric Radiation. Vol. 84, Academic Press.

[28] Myhre, G., *et al*. (2013) Anthropogenic and Natural Radiative Forcing. In: *Climate Change* 2013: *The Physical Science Basis*. *Contribution of Working Group I to the Fifth Assessment Report of the Intergovernmental Panel on Climate Change*, Cambridge University Press, 659-740.

[29] Petty, G.W. (2006) A First Course in Atmospheric Radiation. Sundog Publishing.

[30] Hammel, E., Steiner, M., Marvan, C., Marvan, M., Retzlaff, K., Bergholz, W., *et al*. (2024) CO_2 Back-Radiation Sensitivity Studies under Laboratory and Field Conditions. *Atmospheric and Climate Sciences*, **14**, 407-428. https://doi.org/10.4236/acs.2024.144025